


Article

Synthesis and Characterization of High-Energy *Anti*-Perovskite Compounds $\text{Cs}_3\text{X}[\text{B}_{12}\text{H}_{12}]$ Based on Cesium Dodecahydro-*Closo*-Borate with Molecular Oxoanions ($\text{X}^- = [\text{NO}_3]^-$, $[\text{ClO}_3]^-$ and $[\text{ClO}_4]^-$)

Rouzbeh Aghaei Hakkak, Ioannis Tiritiris and Thomas Schleid * 

Institute for Inorganic Chemistry, University of Stuttgart, D-70569 Stuttgart, Germany; rouzbeh.aghaei-hakkak@iac.uni-stuttgart.de (R.A.H.); tiritiris@iac.uni-stuttgart.de (I.T.)

* Correspondence: schleid@iac.uni-stuttgart.de

Abstract: Three novel *anti*-perovskite compounds, formulated as $\text{Cs}_3\text{X}[\text{B}_{12}\text{H}_{12}]$ ($\text{X}^- = [\text{NO}_3]^-$, $[\text{ClO}_3]^-$, and $[\text{ClO}_4]^-$), were successfully synthesized through the direct mixing of aqueous solutions containing $\text{Cs}_2[\text{B}_{12}\text{H}_{12}]$ and CsX ($\text{X}^-: [\text{NO}_3]^-$, $[\text{ClO}_3]^-$, $[\text{ClO}_4]^-$), followed by isothermal evaporation. All three compounds crystallize in the orthorhombic space group *Pnma*, exhibiting relatively similar unit-cell parameters (e.g., $\text{Cs}_3[\text{ClO}_3][\text{B}_{12}\text{H}_{12}]$: $a = 841.25(5)$ pm, $b = 1070.31(6)$ pm, $c = 1776.84(9)$ pm). The crystal structures were determined using single-crystal X-ray diffraction, revealing a distorted hexagonal *anti*-perovskite order for each. Thermal analysis indicated that the placing oxidizing anions X^- into the $3\text{Cs}^+ + [\text{B}_{12}\text{H}_{12}]^{2-}$ blend leads to a reduction in the thermal stability of the resulting *anti*-perovskites $\text{Cs}_3\text{X}[\text{B}_{12}\text{H}_{12}]$ as compared to pure $\text{Cs}_2[\text{B}_{12}\text{H}_{12}]$, so thermal decomposition commences at lower temperatures, ranging from 320 to 440 °C. Remarkably, the examination of the energy release through DSC studies revealed that these compounds are capable of setting free a substantial amount of energy, up to 2000 J/g, upon their structural collapse under an inert-gas atmosphere (N_2). These three compounds represent pioneering members of the first ever *anti*-perovskite high-energy compounds based on hydro-*closo*-borates.

Keywords: *anti*-perovskite structure; hydroborates; high-energy materials; X-ray crystallography



Citation: Aghaei Hakkak, R.; Tiritiris, I.; Schleid, T. Synthesis and Characterization of High-Energy *Anti*-Perovskite Compounds $\text{Cs}_3\text{X}[\text{B}_{12}\text{H}_{12}]$ Based on Cesium Dodecahydro-*Closo*-Borate with Molecular Oxoanions ($\text{X}^- = [\text{NO}_3]^-$, $[\text{ClO}_3]^-$ and $[\text{ClO}_4]^-$). *Molecules* **2024**, *29*, 382. <https://doi.org/10.3390/molecules29020382>

Academic Editor: Yuanfu Chen

Received: 19 December 2023

Revised: 5 January 2024

Accepted: 8 January 2024

Published: 12 January 2024



Copyright: © 2024 by the authors. Licensee MDPI, Basel, Switzerland. This article is an open access article distributed under the terms and conditions of the Creative Commons Attribution (CC BY) license (<https://creativecommons.org/licenses/by/4.0/>).

1. Introduction

The perovskite crystal structure, with its distinctive ABX_3 composition, has long been a focal point in materials science [1] owing to its diverse range of applications, spanning from photovoltaics [2] to superconductors [3]. In recent years, a counterintuitive class of materials, referred to as *anti*-perovskites, has emerged as a promising avenue for scientific exploration [4]. Unlike their traditional perovskite counterparts, *anti*-perovskite materials exhibit a unique crystallographic arrangement, characterized by an inverted cation–anion order. This unconventional configuration imparts distinct electronic, optical, and structural properties, sparking significant interest in harnessing their potential for groundbreaking advancements in various technological domains. The exploration of *anti*-perovskite materials has gained momentum due to their exceptional properties; these materials have demonstrated promise in diverse applications, such as having a high ionic conductivity [5], as well as opto-electronic [6], catalytic [7] and thermoelectric applications [8].

Boron (B) as a non-metal fuel has garnered considerable attention in advanced solid propellants. With a mass calorific value of up to 58.7 MJ/kg [9,10], boron surpasses another typical metal fuel, such as aluminum (Al), by almost two times, since aluminum has a calorific value of 30.8 MJ/kg. Moreover, the volumetric calorific value of boron reaches an impressive 135.2 kJ/cm³, significantly exceeding that of Al (83.3 kJ/cm³) by 51.9 kJ/cm³ [11,12]. Boron-based, fuel-rich propellants typically comprise the non-metal

fuel boron, oxidants, binders, and additives. Serving as the pivotal component in propellants with a high mass ratio (usually ranging from 25 to 40%), the non-metal fuel boron continues to be a prominent focus in ongoing research [13,14].

On the other hand, hydroborates, notably with the dodecahydro-*closo*-dodecaborate anion $[B_{12}H_{12}]^{2-}$, have been recognized since 1960 [15]. The alkyl-ammonium and alkali-metal compounds and derivatives originating from these hydroborates have captured the attention of numerous researchers owing to their distinctive properties [16]. Alkali and alkaline-earth metal compounds containing the $[B_{12}H_{12}]^{2-}$ anion have exhibited outstanding stability over a wide temperature range. As an example, $Cs_2[B_{12}H_{12}]$ with an *anti*-fluorite structure arrangement remains in a solid and stable state up to temperatures of approximately 800 °C [17].

Anti-perovskites incorporating the dodecahydro-*closo*-dodecaborate anion $[B_{12}H_{12}]^{2-}$ have been previously synthesized, with a number of examples including $Cs_3Cl[B_{12}H_{12}]$, $(NH_4)_3Br[B_{12}H_{12}]$ [18], $K_3I[B_{12}H_{12}]$ [19], $Cs_3[BH_4][B_{12}H_{12}]$ [20], and luminescent $Tl_3Cl[B_{12}H_{12}]$ [21]. Among these compounds, only $Tl_3Cl[B_{12}H_{12}]$ exhibits a hexagonal and not a cubic *anti*-perovskite structure.

Energetic materials are one of the main topics in chemistry, because of their wide range of application as explosives [22], propellants [23] and pyrotechnic materials [24]. Boron-cluster compounds, specifically $[B_{12}H_{12}]^{2-}$ -containing ones, have become a remarkable subject of energetic research. The increased stability of these compounds compared to other borates, coupled with their substantial hydrogen and boron content, positions them at the forefront of energetic investigations. The amalgamation of the $[B_{12}H_{12}]^{2-}$ anion with energetic yet less stable cations has led to the creation of energetic salts, exemplified by diguanidinium [25] and dihydrazinium salts [26]. Under inert atmospheres like N_2 , dihydrazinium salts have demonstrated the capacity to release approximately 1650 J/g of heat next to elemental hydrogen (H_2). Meanwhile, the combustion of diguanidinium salts has been shown to unleash an extraordinary amount of energy, reaching up to 34 kJ/g [27].

Perovskite chemistry recently advanced itself toward the synthesis of new types of energetic materials. A variety of different types of these energetic perovskites were synthesized with different compositions, such as compounds based on inorganic [28] and organic materials [29,30]. These compounds mostly use oxidizing anions, such as perchlorate, on their *X*-site in an ABX_3 perovskite, but there is no record of energetic *anti*-perovskites to date.

In this research, we focused on the synthesis of the first ever high-energy *anti*-perovskite compounds and add new members to this family of high energetic materials. Three novel *anti*-perovskite compounds, namely $Cs_3[NO_3][B_{12}H_{12}]$ (I), $Cs_3[ClO_3][B_{12}H_{12}]$ (II) and $Cs_3[ClO_4][B_{12}H_{12}]$ (III), were successfully synthesized and comprehensively characterized using various methods, include X-ray, single-crystal structure analysis, vibrational spectroscopy (Raman), thermogravimetry (TG), and differential scanning calorimetry (DSC).

2. Results and Discussion

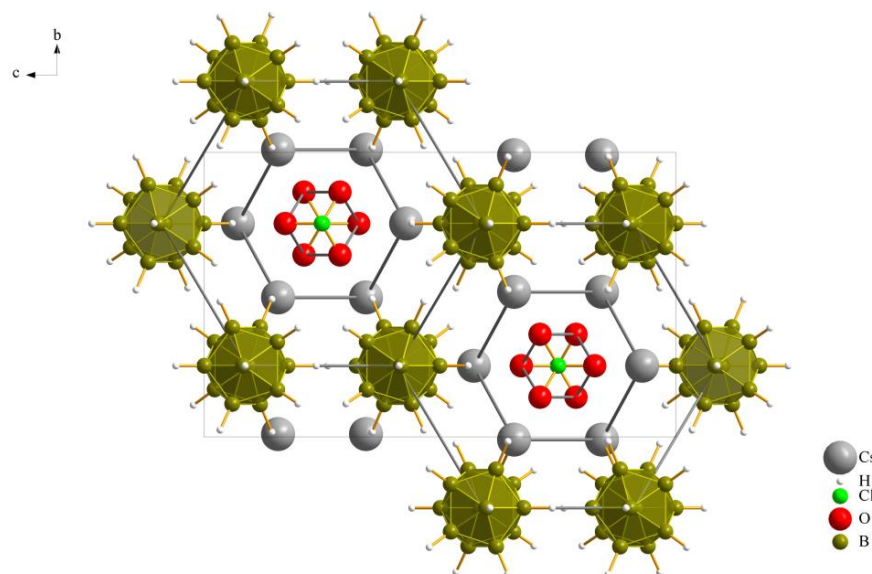
2.1. Crystallography

The three new compounds $Cs_3X[B_{12}H_{12}]$ crystallize similarly in the orthorhombic space group $Pnma$ with four formula units per unit cell and have similar cell parameters. Details of the crystallographic data and their determination are provided in Table 1 and an overall look at the unit cell of $Cs_3[ClO_3][B_{12}H_{12}]$ (II), as an example, is depicted in Figure 1.

In these three compounds under consideration, four distinct molecular polyatomic anions are present: nitrate $[NO_3]^-$, chlorate $[ClO_3]^-$, perchlorate $[ClO_4]^-$ and dodecahydro-*closo*-dodecaborate $[B_{12}H_{12}]^{2-}$. Each of these species exhibits standard bond lengths and angles. Specifically, for nitrate, chlorate and perchlorate, the N–O and Cl–O distances and angles fall within the approximate ranges of 125–127 pm and 118–119°, 146–147 pm and 107–108°, and 141–145 pm and 109–110°, respectively [31–33]. Additionally, the B–B bond lengths within the $[B_{12}H_{12}]^{2-}$ anions typically range between 174 and 181 pm, and are consistently observed [25,26] for all three cases, and the same holds for the B–H distances (108–117 pm).

Table 1. Crystallographic data for the crystal structures of Cs₃[NO₃][B₁₂H₁₂] (I), Cs₃[ClO₃][B₁₂H₁₂] (II) and Cs₃[ClO₄][B₁₂H₁₂] (III).

Compound	Cs ₃ [NO ₃][B ₁₂ H ₁₂] (I)	Cs ₃ [ClO ₃][B ₁₂ H ₁₂] (II)	Cs ₃ [ClO ₄][B ₁₂ H ₁₂] (III)
temperature, K	293	293	293
crystal system	orthorhombic	orthorhombic	orthorhombic
space group	<i>Pnma</i>	<i>Pnma</i>	<i>Pnma</i>
<i>a</i> , pm	848.51(5)	841.25(5)	892.46(5)
<i>b</i> , pm	1045.62(6)	1070.31(6)	1054.89(6)
<i>c</i> , pm	1761.38(9)	1776.84(9)	1718.53(9)
<i>D</i> _{cal} , g cm ⁻³	2.561	2.591	2.627
μ (MoK α), mm ⁻¹	6.95	6.95	6.88
<i>F</i> (000), e ⁻	1072	1112	1144
<i>hkl</i> range	12, 15, 25	10, 13, 22	11, 13, 22
<i>2</i> θ _{max} , deg	31.51	27.48	27.48
refl. measured	31,742	27,436	29,173
refl. unique	2730	1929	1956
<i>R</i> _{int} / <i>R</i> _{σ}	0.064, 0.026	0.117, 0.042	0.055, 0.021
<i>R</i> ₁ / <i>wR</i> ₂	0.042, 0.116	0.050, 0.095	0.022, 0.048
GooF	1.085	1.061	1.088
CSD number	2314128	2313882	2313868

**Figure 1.** Extended unit cell content of the crystal structure of Cs₃[ClO₃][B₁₂H₁₂] (II) as viewed along [100].

In all three compounds, the *quasi*-icosahedral [B₁₂H₁₂]²⁻-cluster units are bisected by both a mirror plane and a glide plane perpendicular to each other. All Cs⁺ cations exhibit a consistent placement on glide planes, while the (Cs1)⁺ cations, in addition to the glide planes, also reside on a mirror plane. Likewise, nitrogen and chlorine within these compounds undergo this bisection using a perpendicular mirror and glide planes.

As previously noted, these compounds exhibit a unique combination reminiscent of the *anti*-perovskite A₃XB structure (A⁺ = Cs⁺, X⁻ = [NO₃]⁻, [ClO₃]⁻ and [ClO₄]⁻, B²⁻ = [B₁₂H₁₂]²⁻). However, it is noteworthy that, despite this association, the crystalline arrangement observed conforms to the hexagonal *anti*-perovskite pattern in all cases. In this specific configuration, the complex molecular oxoanions occupying the X⁻ site are enveloped by six cations from the A⁺ site, forming infinite pillars in the present compounds by sharing *trans*-oriented faces. These pillars are parallel to the crystallographic [100] axis,

as an example this arrangement in compound (I), as depicted in Figure 2, and are bundled like the hexagonal close packing of rods, as emphasized in Figure 1 for compound (II).

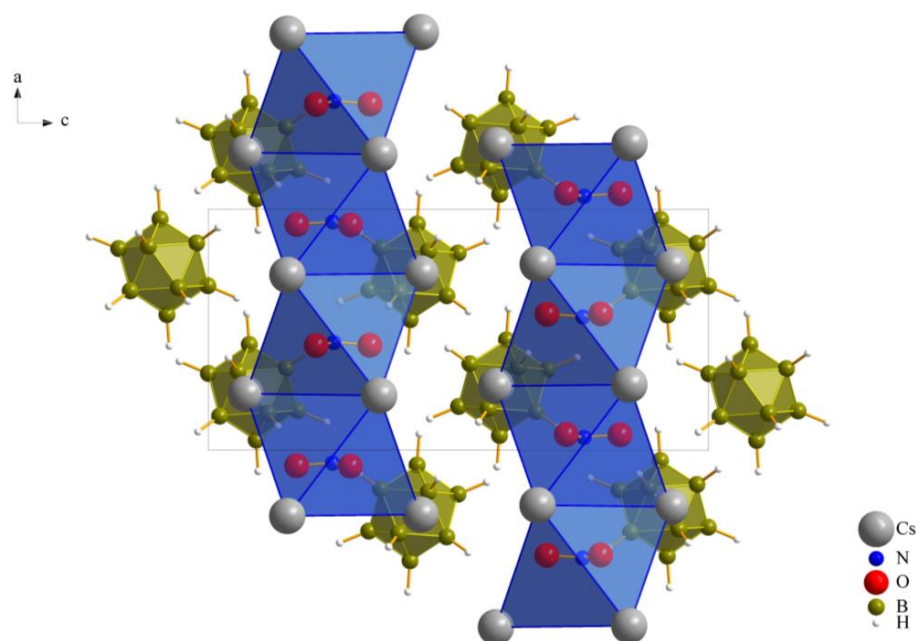


Figure 2. Hexagonal *anti*-perovskite ordering of $\text{Cs}_3[\text{NO}_3][\text{B}_{12}\text{H}_{12}]$ (I) as viewed along [010].

The monovalent molecular anions, nitrate, chlorate and perchlorate, exhibit a distinctive three-dimensional positioning within the octahedral coordination environment with Cs^+ cations (two $(\text{Cs}1)^+$ and four $(\text{Cs}2)^+$), leading to their considerable structural resemblance. Our initial prediction for nitrate $[\text{NO}_3]^-$, based on its triangular planar two-dimensional shape, differed from that for chlorate and perchlorate, both featuring three-dimensional shapes (trigonal pyramidal and tetrahedral, respectively). However, the key to their similarity lies within the octahedral Cs^+ -cation arrangement. As illustrated in Figure 3, the nitrate anion is not centrally located within this octahedron, neither parallel nor perpendicular to the square. Instead, it assumes an oblique position. The standard deviation percentages (SDP) for compounds (I), (II) and (III) are 4.52, 1.13 and 1.12, respectively. These values suggest that chlorate and perchlorate can realize nearly ideal $(\text{Cs}^+)_6$ octahedra around them. In contrast, nitrate introduces a subtle distortion to the octahedral geometry. This nuanced distortion emphasizes the intricacies associated with the positioning of the nitrate anion within the crystal structure, contributing to the slight structural variations observed among the three compounds.

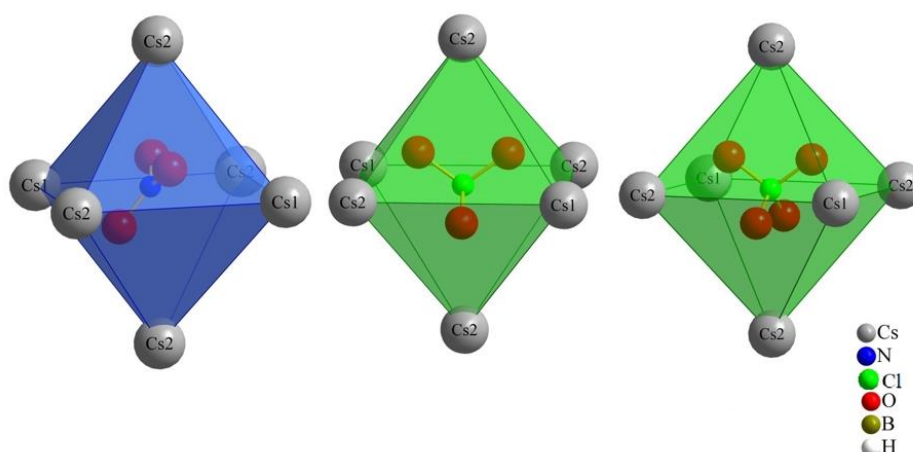


Figure 3. Orientation of the monovalent oxoanions in compounds (I), (II) and (III).

The coordination sphere around the Cs^+ cations for both Cs1 and Cs2 in all three compounds consists of twelve (or even more) atoms, which is similar to the “normal” coordination numbers for the *A* site in cubic or hexagonal ABX_3 perovskites. The cesium cations (1 and 2) are surrounded by two monovalent oxoanions (nitrate, chlorate and perchlorate) and four divalent anions ($[\text{B}_{12}\text{H}_{12}]^{2-}$) with a *cis*-orientation, so the cesium cations are connected with two bonds and one bond to the oxygen atoms of the monovalent anions, and with one triple contact and three double contacts to surrounding boron cluster anions $[\text{B}_{12}\text{H}_{12}]^{2-}$.

The coordination environment around both Cs^+ cations (Cs1 and Cs2) in all three compounds is consistent with a coordination number of 12 and aligns well with the typical coordination numbers for perovskites (Figures 4 and 5).

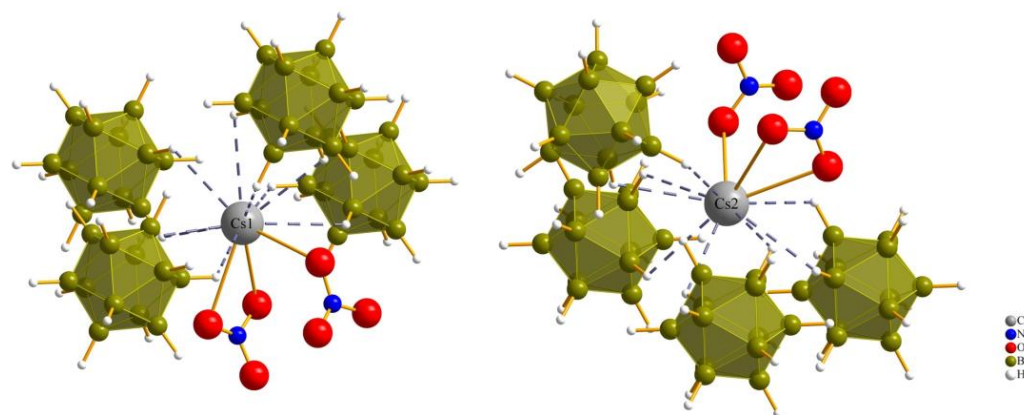


Figure 4. Anionic coordination spheres around $(\text{Cs1})^+$ and $(\text{Cs2})^+$ in $\text{Cs}_3[\text{NO}_3][\text{B}_{12}\text{H}_{12}]$ (I).

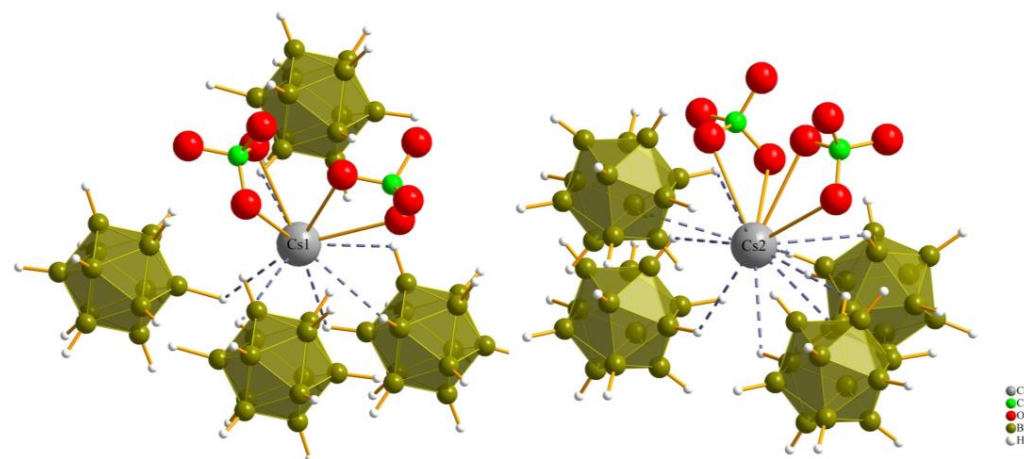


Figure 5. Anionic coordination spheres around $(\text{Cs1})^+$ and $(\text{Cs2})^+$ in $\text{Cs}_3[\text{ClO}_4][\text{B}_{12}\text{H}_{12}]$ (III).

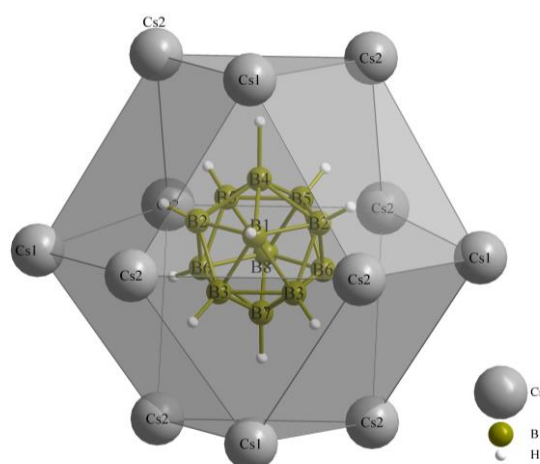
For compound (III), each of the cesium cations is connected again to two perchlorate anions and four boron-cluster anions, but in this compound each anion has two instances of contact with each cesium cation to add up to the coordination number of 12 (Figure 5).

Both kinds of cesium cations establish two bidentate Cs–O contacts to two monovalent perchlorate oxoanions, while $(\text{Cs1})^+$ is connected to four boron-cluster anions with different numbers of Cs–H contacts to each, with one monodentate, two bidentate and one tridentate contact and, for $(\text{Cs2})^+$, the number of Cs–H contacts to the four neighboring boron-cluster anions is ordered differently. Two monodentate and two bidentate contacts are used to complete the *anti*-perovskite twelvefold coordination for this position too. The interatomic distances for Cs–H and Cs–O bonds are listed in Table 2.

Table 2. Cs–O and Cs–H bond lengths in compounds (I), (II) and (III).

Compound	Cs–O Bond Lengths (d/pm)	Cs–H Bond Lengths (d/pm)
Cs ₃ [NO ₃][B ₁₂ H ₁₂] (I)	310–320	313–359
Cs ₃ [ClO ₃][B ₁₂ H ₁₂] (II)	318–327	307–355
Cs ₃ [ClO ₄][B ₁₂ H ₁₂] (III)	316–330	311–357

Figure 6 illustrates the *anti*-cuboctahedron $\{[B_{12}H_{12}](Cs1)_4(Cs2)_8\}^{10+}$, which is formed by the mixed hexagonal close packing of Cs⁺ cations and $[B_{12}H_{12}]^{2-}$ anions. This arrangement follows the $\frac{3}{\infty}\{([B_{12}H_{12}]Cs_{12/4})^+\}$ structure, which is suitable for hosting X⁻-anion chains along [100], embedded into $\frac{1}{\infty}\{[XC_{s6/2}]^{2+}\}$ pillars.

**Figure 6.** *Anti*-cuboctahedron $\{[B_{12}H_{12}](Cs1)_4(Cs2)_8\}^{10+}$ as result of the mixed hexagonal close packing of Cs⁺ cations and $[B_{12}H_{12}]^{2-}$ anions.

Despite its structure description and the cubic close packing of $[B_{12}H_{12}]^{2-}$ anions with Cs⁺ cations in all tetrahedral voids, the *anti*-fluorite arrangement of Cs₂[B₁₂H₁₂] ($V_m = 216.15 \text{ cm}^3/\text{mol}$) appears rather fluffy. Therefore, the formation of double salts with the composition Cs₃X[B₁₂H₁₂] is regarded as having derived from the *pseudo*-binaries CsX and Cs₂[B₁₂H₁₂], and always occurs under densification when compared to the sum of their molar volumes ($\Sigma = V_m(\text{Cs}_2[\text{B}_{12}\text{H}_{12}]) + V_m(\text{CsX})$; see Table 3). Even the formation of the dihydrate Cs₂[B₁₂H₁₂] · 2 H₂O matches this scheme.

Table 3. Molar volumes (V_m in $\text{cm}^3 \cdot \text{mol}^{-1}$) of compounds (I) to (III), their precursor materials, and similar hydro-borate perovskites, with a comparison of the calculated sum of the components and the real values. $V_m(\text{B})$ represents $V_m(\text{Cs}_2[\text{B}_{12}\text{H}_{12}])$, and $V_m(\text{C})$ represents $V_m(\text{CsX})$ or V_m (ice-I), respectively.

Compound A	$V_m(\text{A})$	$V_m(\text{B}) + V_m(\text{C})$	$V_m(\text{B or C})$	Component B and C
–	–	–	216.2	Cs ₂ [B ₁₂ H ₁₂] [19] (B)
Cs ₃ [NO ₃][B ₁₂ H ₁₂]	235.3	270.4	54.2	Cs[NO ₃] [34] (C)
Cs ₃ [ClO ₃][B ₁₂ H ₁₂]	240.9	273.1	56.9	Cs[ClO ₃] [35] (C)
Cs ₃ [ClO ₄][B ₁₂ H ₁₂]	243.6	275.5	69.3	Cs[ClO ₄] [36] (C)
Cs ₃ Cl[B ₁₂ H ₁₂] [18]	220.8	258.3	42.1	CsCl [37] (C)
Cs ₃ Br[B ₁₂ H ₁₂] [18]	224.8	263.2	47.0	CsBr [38] (C)
Cs ₃ I[B ₁₂ H ₁₂] [18]	236.9	273.4	57.2	CsI [39] (C)
Cs ₂ [B ₁₂ H ₁₂] · 2 H ₂ O [40]	202.0	254.2	19.0	H ₂ O (ice-I) [41] (C)

The Goldschmidt tolerance factor is a widely employed tool to assess the stability of perovskites, calculated using the formula $t_G = (r_B + r_A) / \sqrt{2}(r_X + r_A)$, where r_A , r_B , and r_X represent the ionic radii of A, B, and X, respectively, and an ideal perovskite ABX_3

has a tolerance factor of 1 [21]. Calculating the Goldschmidt tolerance factors (t_G) with $r([B_{12}H_{12}]^{2-}) = 322$ pm, $r(Cs^+) = 177$ [21], and $r([NO_3]^-)$, $r([ClO_3]^-)$ and $r([ClO_4]^-)$ as 200, 208 and 225 [42], respectively, yields values of 0.936, 0.917 and 0.878 for compounds (I)–(III), respectively. These values fall within a narrow range, indicating a trend that aligns with predictions for the same perovskite-type structure, but not the hexagonal one. This seems to be often the case for *anti*-perovskite-type cesium compounds and was previously stated for Cs_3OCl [43], Cs_3OBr , Cs_3OI [44] and $Cs_3O Au$ [45], where O^{2-} plays the role of X^- and Cl^- takes the $[B_{12}H_{12}]^{2-}$ part.

2.2. Raman Spectroscopy

Raman spectroscopy was executed on powder samples of the compounds (I), (II) and (III). All three compounds exhibit similarities in four distinct regions associated with the vibrational characteristics of the dianionic boron cluster $[B_{12}H_{12}]^{2-}$. In the spectral range spanning from 2500 to 2400 cm^{-1} , a distinct manifestation of the symmetric breathing vibration of the boron cage becomes apparent. This phenomenon is predominantly influenced by the stretching mode of B–H bonds. Notably, the cubic $Cs_2[B_{12}H_{12}]$ crystals in the space group $Fm\bar{3}$ [46] show only one peak in the specified region. Intriguingly, when the compound symmetry is diminished to orthorhombic in the space group $Pnma$, a unique outcome emerges—the region undergoes splitting, introducing a distinctive spectral pattern [21]. Accordingly, the anticipated finding is the observation of just two discernible peaks. Another marked region, spanning from 950 to 920 cm^{-1} , corresponds to B–B stretching vibrations. At 750 cm^{-1} , the most intense peak signifies the symmetric breathing mode of the B_{12} cage, while the interval from 570 to 560 cm^{-1} can be ascribed to more B–B stretching vibrations, culminating in lattice vibrations at approximately 200 cm^{-1} .

In the case of compound (I), a subtle peak at 1350 cm^{-1} is discernible, which is attributable to the asymmetric stretch of the nitrate group. Notably, an intense symmetric stretching mode of the nitrate anion can be observed around 1050 cm^{-1} , accompanied by a less pronounced peak at 700 cm^{-1} , corresponding to its in-plane deformation mode. For compounds (II) and (III), distinctive features emerge, including three regions at 950 cm^{-1} associated with symmetric Cl–O stretching (overlapping with B–B skeleton vibrations), and wavenumbers of 620 and 470 cm^{-1} , indicative of the active and inactive deformations of the Cl–O bonds, respectively [47]. As an example, the Raman spectrum of compound (II) is depicted in Figure 7, and the Raman spectra of compounds (I) and (III) are available as Figures S1 and S2 in the Supplementary Material.

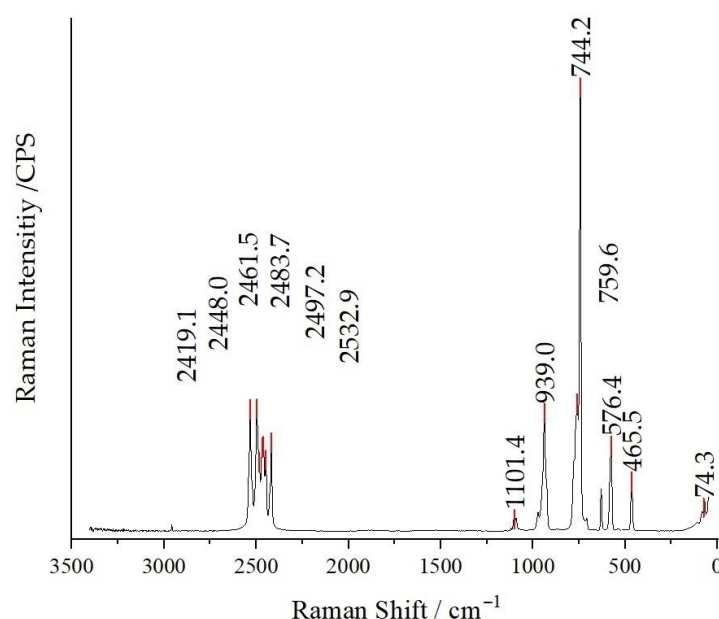


Figure 7. Raman spectrum of $Cs_3[ClO_3][B_{12}H_{12}]$ (II) recorded at an excitation wavelength of $\lambda = 740$ nm.

2.3. Thermal Analysis

Two distinct methods of thermal analyses, namely TG/DTA and DSC, were conducted for the three compounds under investigation. The TG analysis revealed that the thermal decomposition of these compounds occurs at significantly lower temperatures when compared to the pure cesium salt of $[B_{12}H_{12}]^{2-}$, namely cubic $Cs_2[B_{12}H_{12}]$. In terms of mass loss, compound (I) exhibits a single-step thermal decomposition with an onset point at approximately 440 °C, resulting in a 3% mass loss (Figure 8). Conversely, compounds (II) and (III) undergo thermal decomposition in two closely spaced steps, each with less than 1% mass loss for both. The onset points for these steps are 360 °C for compound (II) and 320 °C for compound (III). The mass loss for these compounds initiates at substantially lower temperatures compared to $Cs_2[B_{12}H_{12}]$, which decomposes at around 800 °C.

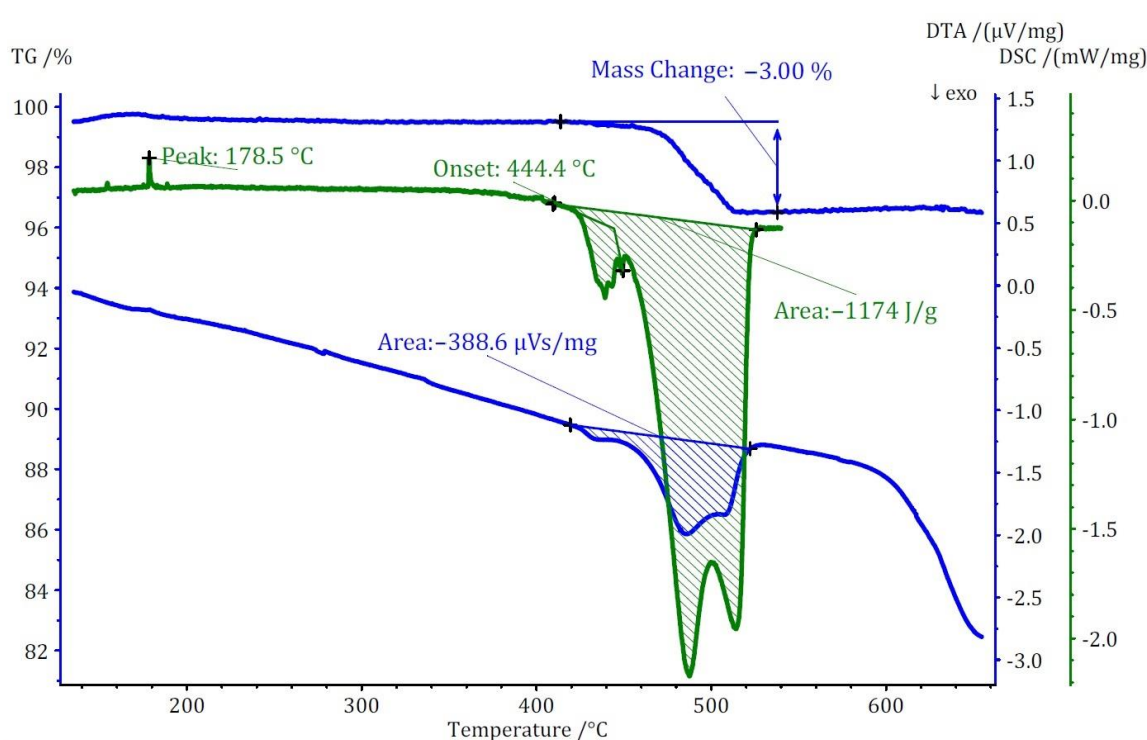


Figure 8. Thermoanalytical TG/DTA and DSC diagram of $Cs_3[NO_3][B_{12}H_{12}]$ (I).

The thermal study of these compounds also revealed intriguing energetic properties, particularly through their DSC analyses. Compound (I) exhibits a small endothermic peak around 180 °C, likely associated with a phase transition due to there being no observable mass change at this temperature. Subsequently, a substantial exothermic peak emerges at around 440 °C with an area of -1175 J/g. For compound (II), an endothermic peak appears at a remarkably low temperature of around 90 °C, followed by two consecutive exothermic peaks. The first exothermic peak has an area of approximately 800 J/g. Unfortunately, the DSC analysis could not be extended beyond 550 °C due to the crucible limitations. However, by comparing DTA and DSC numbers for the first peak, the area of the second peak was estimated to be approximately -360 J/g. Collectively, compound (II) exhibits an energy release of around 1150 J/g in two steps. In the case of compound (III), two endothermic peaks without a change in mass are observed at around 206 and 306 °C, followed by one substantial and one small exothermic peak. The first exothermic peak is observable in both DSC and DTA analyses with an energy release of around 1750 J/g. The second peak, detectable only in the DTA analysis, has an estimated energy release of around 200 J/g, resulting in a total energy release of approximately 1950 J/g (Figure 9). The observed phase transitions at lower temperatures align with findings from prior thermal studies on similar $[B_{12}H_{12}]^{2-}$ -containing compounds [10,11]. Earlier investigations into $Cs_2[B_{12}H_{12}]$ [17]

demonstrated the remarkable stability of the cesium salt, maintaining its structural integrity up to approximately 800 °C, and, during the thermal decomposition, a singular endothermic peak was identified. However, the addition of oxidizing anions into the compound induced a notable shift, causing decomposition to initiate at far lower temperatures. This deviation from the behavior of simple salts was marked by the emergence of strongly exothermic decomposition reactions.

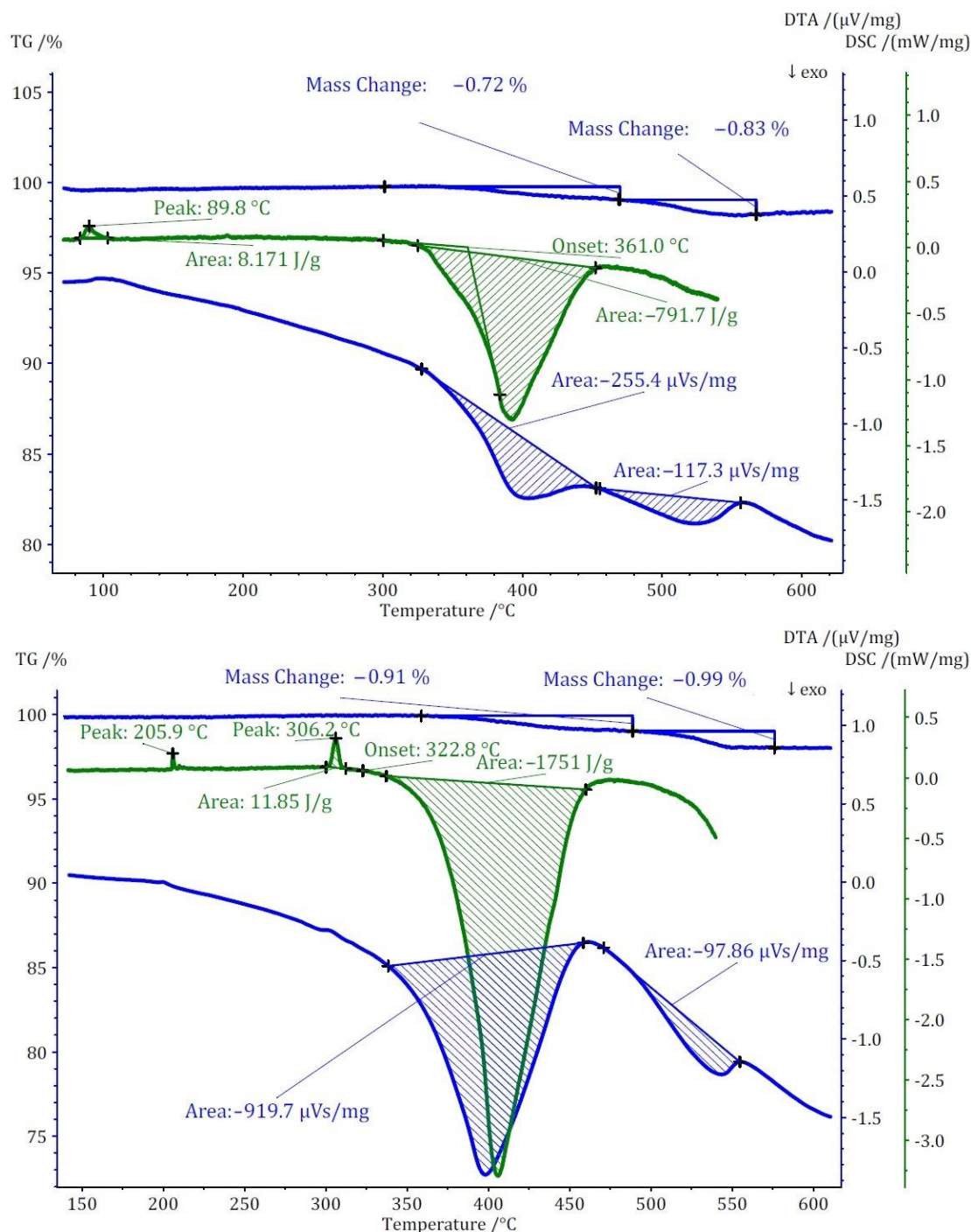


Figure 9. Thermoanalytical TG/DTA and DSC diagrams of $\text{Cs}_3[\text{ClO}_3][\text{B}_{12}\text{H}_{12}]$ (II) (top) and $\text{Cs}_3[\text{ClO}_4][\text{B}_{12}\text{H}_{12}]$ (III) (bottom).

The decomposition temperatures of these three compounds exceed those of traditional energetic materials by far, rendering them exceptionally thermally stable. Notably, the heat release of compound (III) is nearly equivalent to that one of 1,3,5,7-tetranitro-

1,3,5,7-tetrazocane (HMX, 1987 J/g). Refer to Table 4 for a comprehensive depiction of the decomposition temperatures of compounds (I)–(III) alongside the traditional high-energy materials and their density [48]. Density is a pivotal parameter in the high-energy materials domain and a higher density always favors these materials due to their lower space consumption and increased ratio of energy per volumetric space. The density of compounds (I) to (III) are relatively equal, ranging from 2.56 to 2.69 g·cm^{−3}, respectively, due to their similarity in both unit-cell parameter and molar masses, and they always show a denser packing in comparison to pure Cs₂[B₁₂H₁₂], as mentioned in a previous section.

Table 4. Decomposition temperatures of compounds (I)–(III) as compared to some traditional energetic materials and a compilation of their densities.

Compound	Decomposition Peak (°C)	Density (g·cm ^{−3})
Cs ₂ [B ₁₂ H ₁₂]	800	1.43
Cs ₃ [NO ₃][B ₁₂ H ₁₂] (I)	440–480–514	2.56
Cs ₃ [ClO ₃][B ₁₂ H ₁₂] (II)	393	2.59
Cs ₃ [ClO ₄][B ₁₂ H ₁₂] (III)	405	2.63
Hexahydro-1,3,5-trinitro-1,3,5-triazine (RDX)	210	1.82
1,3,5,7-Tetranitro-1,3,5,7-tetrazocane (HMX)	283	1.91
2,4,6-Trinitrotoluene (TNT)	290	1.65

3. Materials and Methods

3.1. Synthesis

The three *anti*-perovskite compounds featuring dodecahydro-*closo*-dodecaborate anions were synthesized by dissolving Cs₂[B₁₂H₁₂] (ABCR (Karlsruhe, Germany)) in a minimal amount of distilled water. Subsequently, a 1:1 ratio of appropriate cesium salts (cesium nitrate: Sigma Aldrich (St. Louis, MO, USA), cesium chlorate: mixture of sodium chlorate (Fluka (Buchs, Switzerland)) and cesium hydroxide (Sigma Aldrich) and cesium perchlorate: prepared by mixing freshly obtained cesium hydroxide (Sigma Aldrich) with perchloric acid (70%, Fisher Scientific (Hampton, NH, USA))) was added to portions of this solution. The resulting clear brine was subjected to isothermal evaporation at room temperature, yielding transparent and colorless single crystals of the respective salts Cs₃X[B₁₂H₁₂] (X[−] = [NO₃][−], [ClO₃][−] and [ClO₄][−]).

3.2. Devices

3.2.1. X-ray Crystallography

Single-crystal X-ray diffraction data were acquired utilizing a Nonius κ-CCD diffractometer with Mo-Kα radiation graphite-monochromatized to a wavelength of λ = 71.07 pm. The entire process, spanning initial structure solutions via direct methods to subsequent structure refinements, was conducted using the SHELX-97 program package [49,50]. Atomic positions were accurately determined through difference Fourier maps based on the collected data, facilitating the anisotropic refinement of all non-hydrogen atoms. Detailed information regarding the data collection and the outcomes of the final structure refinements is provided in Table 1. Supplementary data related to the structure refinements can be accessed through the Fachinformationszentrum (FIZ) Karlsruhe (D-73644 Eggenstein-Leopoldshafen, E-mail: crysdata@fiz-karlsruhe.de) and are referenced with the numbers outlined in Table 1. Fractional atomic positions are additionally available in Tables S1–S3 of the Supplementary Material. It is noteworthy that, in this study, hydrogen atom positions were ascertained through electron-density maps generated by difference Fourier syntheses utilizing the X-ray diffraction data. No further calculations or corrections were deemed necessary, given that the positions of these hydrogen atoms are well-defined based on their precise angles and distances in relation to other atoms.

3.2.2. Thermal Analysis

Two distinct instruments were employed for thermal analyses in this study. The first device, STA 449 C Jupiter by Netzsch (Selb, Germany) with alumina crucibles, played a crucial role in the investigation. TG analysis was carried out in alumina crucibles with a heat rate of 5 K min⁻¹ under an argon atmosphere. The second device, DSC 201, also from Netzsch, operated as a differential scanning calorimeter with a heating rate of 5 K min⁻¹ and a nitrogen flow of 20 mL min⁻¹ and samples prepared in aluminum crucibles with a maximum temperature of 600 °C. This instrument was essential in the research, providing precise measurements of the various thermal properties of the samples. These properties encompassed heat capacity, energy changes and activation energies, all of which were indispensable for the comprehensive analysis conducted in the study.

3.2.3. Raman Spectroscopy

We performed Raman spectroscopic analyses with the DXR Smart Raman system, a product developed by Thermo Fisher (Waltham, MA, USA), which operates at an excitation wavelength of $\lambda = 740$ nm. The spectroscopic data collected during these analyses were meticulously scrutinized.

4. Conclusions

The synthesis of three novel *anti*-perovskite compounds, Cs₃X[B₁₂H₁₂] ($X^- = [\text{NO}_3]^-$, $[\text{ClO}_3]^-$, $[\text{ClO}_4]^-$), is presented in this research. These compounds exhibit orthorhombic crystal structures in the space group *Pnma*, with comparable unit-cell parameters. Single-crystal X-ray diffraction has unveiled a hexagonal *anti*-perovskite order for each compound, characterized by pillars $\frac{1}{\infty} \{[\text{XC}_6\text{O}_6]^{2+}\}$ of *trans*-faced connected $[\text{XC}_6\text{O}_6]^{5+}$ octahedra, which are bundled like a hexagonal close rod packing, held together by *quasi*-icosahedral $[\text{B}_{12}\text{H}_{12}]^{2-}$ anions with a counter-intuitive Goldschmidt tolerance factor far below 1. Thermal analyses have revealed a reduction in thermal stability as compared to Cs₂[B₁₂H₁₂], with decomposition processes commencing at lower temperatures (from 320 to 440 °C) upon the introduction of oxidizing anions. Additionally, differential scanning calorimetry (DSC) has indicated that the presence of molecular oxoanions in the compounds leads to an exceptional energy release potential, reaching up to 2000 J/g, as the compounds undergo structural collapse in an inert-gas atmosphere (N₂). The substantial energy release and elevated decomposition characteristics render these compounds promising candidates for thermally stable energetic materials. This pioneering advancement solidifies their significance in the domain of energetic *anti*-perovskite materials.

Supplementary Materials: The following supporting information can be downloaded at: <https://www.mdpi.com/article/10.3390/molecules29020382/s1>, Table S1. Atomic coordinates and coefficients of the equivalent isotropic displacement parameters for Cs₃[NO₃][B₁₂H₁₂] (I); Table S2. Atomic coordinates and coefficients of the equivalent isotropic displacement parameters for Cs₃[ClO₃][B₁₂H₁₂] (II); Table S3. Atomic coordinates and coefficients of the equivalent isotropic displacement parameters for Cs₃[ClO₄][B₁₂H₁₂] (III); Figure S1. Raman spectrum of Cs₃[NO₃][B₁₂H₁₂] (I); Figure S2. Raman spectrum of Cs₃[ClO₄][B₁₂H₁₂] (III).

Author Contributions: Research, analysis: R.A.H. and I.T.; writing: R.A.H.; supervision, correction: T.S. All authors have read and agreed to the published version of the manuscript.

Funding: The Federal State of Baden-Württemberg.

Data Availability Statement: CIF files are available at the CSD database. Other raw files are not necessary, and all the diagram and picture represent in article file and the Supplementary Material.

Acknowledgments: We would also like to express our gratitude to Falk Lissner from the academic staff of the University of Stuttgart for measuring single crystals and to Christof Schneck, chemical technical assistant at the Institute of Inorganic Chemistry of University of Stuttgart, for helping and providing us with insights to obtain better and more accurate thermal analysis results.

Conflicts of Interest: The authors declare no conflicts of interest.

References

1. Arul, N.S.; Nithya, V.D. *Revolution of Perovskite*; Springer: Singapore, 2020.
2. Park, N.G. Halide Perovskite Photovoltaics: History, Progress, and Perspectives. *MRS Bull.* **2018**, *43*, 527–533. [[CrossRef](#)]
3. Han, J.; Zhu, X.; Zhang, J.; Cai, S.; Guo, J.; Zhou, Y.; Zhao, J.; Wang, P.; Wang, L.; Wei, X. Superconducting-Insulating Quantum Phase Transition Associated with Valence Change in Compressed Perovskite Bismuth-Oxides. *arXiv* **2023**, arXiv:2305.08406.
4. Krivovichev, S.V. Minerals with Antiperovskite Structure: A Review. *Z. Kristallogr.* **2008**, *223*, 109–113. [[CrossRef](#)]
5. Zhao, Y.; Daemen, L.L. Superionic Conductivity in Lithium-Rich Anti-Perovskites. *J. Am. Chem. Soc.* **2012**, *134*, 15042–15047. [[CrossRef](#)]
6. Ullah, I.; Murtaza, G.; Khenata, R.; Mahmood, A.; Muzzamil, M.; Amin, N.; Saleh, M. Structural and Optoelectronic Properties of X_3ZN ($X = Ca, Sr, Ba$; $Z = As, Sb, Bi$) Anti-Perovskite Compounds. *J. Electron. Mater.* **2016**, *45*, 3059–3068. [[CrossRef](#)]
7. Zhu, Y.; Chen, G.; Zhong, Y.; Chen, Y.; Ma, N.; Zhou, W.; Shao, Z. A Surface-Modified Antiperovskite as an Electrocatalyst for Water Oxidation. *Nat. Commun.* **2018**, *9*, 2326. [[CrossRef](#)]
8. Han, D.; Zhu, B.; Cai, Z.; Spooner, K.B.; Rudel, S.S.; Schnick, W.; Bein, T.; Scanlon, D.O.; Ebert, H. Discovery of Multi-Anion Antiperovskites X_6NFSn_2 ($X = Ca, Sr$) as Promising Thermoelectric Materials by Computational Screening. *Matter* **2023**, *7*, 158–174. [[CrossRef](#)]
9. Ulas, A.; Kuo, K.K.; Gotzmer, C. Ignition and Combustion of Boron Particles in Fluorine-Containing Environments. *Combust. Flame* **2001**, *127*, 1935–1957. [[CrossRef](#)]
10. Chintersingh, K.-L.; Nguyen, Q.; Schoenitz, M.; Dreizin, E.L. Combustion of Boron Particles in Products of an Air-Acetylene Flame. *Combust. Flame* **2016**, *172*, 194–205. [[CrossRef](#)]
11. Cao, W.; Guo, W.; Ding, T.; Han, Y.; Li, M.; Gao, D.; Guo, X. LASER Ablation of Aluminized RDX with Added Ammonium Perchlorate or Ammonium Perchlorate/Boron/Magnesium Hydride. *Combust. Flame* **2020**, *221*, 194–200. [[CrossRef](#)]
12. Dreizin, E.L. Metal-Based Reactive Nanomaterials. *Prog. Energy Combust. Sci.* **2009**, *35*, 141–167. [[CrossRef](#)]
13. Liu, L.; He, G.; Wang, Y. Thermal Reaction Characteristics of the Boron Used in the Fuel-Rich Propellant. *J. Therm. Anal. Calorim.* **2013**, *114*, 1057–1068. [[CrossRef](#)]
14. Mi, X.; Goroshin, S.; Higgins, A.J.; Stowe, R.; Ringuette, S. Dual-Stage Ignition of Boron Particle Agglomerates. *Combust. Flame* **2013**, *160*, 2608–2618. [[CrossRef](#)]
15. Wunderlich, J.A.; Lipscomb, W.N. Structure of $B_{12}H_{12}^{2-}$ Ion. *J. Am. Chem. Soc.* **1960**, *82*, 4427–4428. [[CrossRef](#)]
16. Sivaev, I.B.; Bregadze, V.I.; Sjöberg, S. Chemistry of Closo-Dodecaborate Anion $[B_{12}H_{12}]^{2-}$: A Review. *Collect. Czechoslov. Chem. Commun.* **2002**, *67*, 679–727. [[CrossRef](#)]
17. Tiritiris, I. Untersuchungen zu Reaktivität, Aufbau und Struktureller Dynamik von Salzartigen Closo-Dodekaboraten. Ph.D. Thesis, University of Stuttgart, Stuttgart, Germany, 2004.
18. Tiritiris, I.; Weidlein, J.; Schleid, T. Dodekahydro-closo-Dodekaborat-Halogenide der schweren Alkalimetalle mit der Formel $M_3X[B_{12}H_{12}]$ ($M = K-Cs, NH_4$; $X = Cl$ und Br) / Dodekahydro-closo-Dodekaborate Halides of the Heavy Alkali Metals with the Formula $M_3X[B_{12}H_{12}]$ ($M = K-Cs, NH_4$; $X = Cl$ and Br). *Naturforsch. B* **2005**, *60*, 627–639. [[CrossRef](#)]
19. Tiritiris, I.; Schleid, T. Die Dodekahydro-closo-Dodekaborate $M_2[B_{12}H_{12}]$ der schweren Alkalimetalle ($M^+ = K^+, Rb^+, NH_4^+, Cs^+$) und ihre formalen Iodid-Addukte $M_3I[B_{12}H_{12}]$ ($\equiv MI \cdot M_2[B_{12}H_{12}]$). *Z. Anorg. Allg. Chem.* **2003**, *629*, 1390–1402. [[CrossRef](#)]
20. Schouwink, P.; Sadikin, Y.; van Beek, W.; Černý, R. Experimental Observation of Polymerization from BH_4^- to $B_{12}H_{12}^{2-}$ in Mixed-Anion $A_3BH_4B_{12}H_{12}$ ($A = Rb^+, Cs^+$). *Int. J. Hydrogen Energy* **2015**, *40*, 10902–10907. [[CrossRef](#)]
21. Bareiß, K.U.; Bette, S.; Ensling, D.; Jüstel, T.; Schleid, T. Extraordinary Intense Blue Tl^+ Lone-Pair Photoluminescence from Thallium(I) Chloride Hydroborate $Tl_3Cl[B_{12}H_{12}]$. *Dalton. Trans.* **2022**, *51*, 13331–13341. [[CrossRef](#)]
22. Fischer, D.; Klapötke, T.M.; Stierstorfer, J. 1, 5-Di (Nitramino) Tetrazole: High Sensitivity and Superior Explosive Performance. *Angew. Chem. Int. Ed.* **2015**, *54*, 10299–10302. [[CrossRef](#)] [[PubMed](#)]
23. Klapötke, T.M.; Minar, N.K.; Stierstorfer, J. Investigations of Bis(Methyltetrazolyl) Triazines as Nitrogen-Rich Ingredients in Solid Rocket Propellants—Synthesis, Characterization and Properties. *Polyhedron* **2009**, *28*, 13–26. [[CrossRef](#)]
24. Steinhäuser, G.; Klapötke, T.M. “Green” Pyrotechnics: A Chemists’ Challenge. *Angew. Chem. Int. Ed.* **2008**, *47*, 3330–3347. [[CrossRef](#)]
25. Aghaei Hakkak, R.; Schleid, T. Crystal Structure and Thermal Behavior of Three Potential High-Energy Compounds of Hydro-Closo-Borates with Guanidinium. *J. Solid State Chem.* **2023**, *329*, 124416. [[CrossRef](#)]
26. Zimmermann, L.W.; Aghaei Hakkak, R.; Ranjbar, M.; Schleid, T. Crystal Structures and Thermal Analyses of Three New High-Energy Hydrazinium Hydro-Closo-Borates. *Int. J. Hydrogen Energy* **2024**, *16*, 1469–1477. [[CrossRef](#)]
27. Rao, M.H.; Muralidharan, K. Closo-Dodecaborate ($B_{12}H_{12}$) $^{2-}$ Salts with Nitrogen Based Cations and Their Energetic Properties. *Polyhedron* **2016**, *115*, 105–110. [[CrossRef](#)]
28. Shang, Y.; Chen, S.L.; Yu, Z.H.; Huang, R.K.; He, C.-T.; Ye, Z.-M.; Zhang, W.-X.; Chen, X.-M. Silver(I)-Based Molecular Perovskite Energetic Compounds with Exceptional Thermal Stability and Energetic Performance. *Inorg. Chem.* **2022**, *61*, 4143–4149. [[CrossRef](#)]
29. Zhou, J.; Ding, L.; Zhao, F.; Wang, B.; Zhang, J. Thermal Studies of Novel Molecular Perovskite Energetic Material $(C_6H_{14}N_2)[NH_4(ClO_4)_3]$. *Chin. Chem. Lett.* **2020**, *31*, 554–558. [[CrossRef](#)]
30. Shang, Y.; Huang, R.K.; Chen, S.L.; He, C.T.; Yu, Z.H.; Ye, Z.M.; Zhang, W.X.; Chen, X.M. Metal-Free Molecular Perovskite High-Energetic Materials. *Cryst. Growth Des.* **2020**, *20*, 1891–1897. [[CrossRef](#)]

31. Abrahams, S.C.; Bernstein, J.L. Remeasurement of Optically Active NaClO₃ and NaBrO₃. *Acta Crystallogr.* **1977**, *B33*, 3601–3604. [[CrossRef](#)]
32. Sass, R.L.; Vidale, R.; Donohue, J. Interatomic Distances and Thermal Anisotropy in Sodium Nitrate and Calcite. *Acta Crystallogr.* **1957**, *10*, 567–570. [[CrossRef](#)]
33. Fugel, M.; Malaspina, L.A.; Pal, R.; Thomas, S.P.; Shi, M.W.; Spackman, M.A.; Sugimoto, K.; Grabowsky, S. Revisiting a Historical Concept by Using Quantum Crystallography: Are Phosphate, Sulfate and Perchlorate Anions Hypervalent? *Chem. Eur. J.* **2019**, *25*, 6523–6532. [[CrossRef](#)]
34. Lucas, B.W. The Structure (Neutron) of Phase II Caesium Nitrate at 298 K, CsNO₃. *Acta Crystallogr.* **1983**, *C39*, 1591–1594. [[CrossRef](#)]
35. Griesemer, S.D.; Ward, L.; Wolverton, C. High-Throughput Crystal Structure Solution Using Prototypes. *Phys. Rev. Mater.* **2021**, *5*, 105003. [[CrossRef](#)]
36. Granzin, J. Refinement of the Crystal Structures of RbClO₄ and CsClO₄. *Z. Kristallogr.* **1988**, *184*, 157–160. [[CrossRef](#)]
37. Sist, M.; Fischer, K.F.F.; Kasai, H.; Iversen, B.B. Low-Temperature Anharmonicity in Cesium Chloride (CsCl). *Angew. Chem. Int. Ed.* **2017**, *56*, 3625–3629. [[CrossRef](#)]
38. Demont, A.; Prestipino, C.; Hernandez, O.; Elkaïm, E.; Paofai, S.; Naumov, N.; Fontaine, B.; Gautier, R.; Cordier, S. Unprecedented Electron-Poor Octahedral Ta₆ Clusters in a Solid-State Compound: Synthesis, Characterisations and Theoretical Investigations of Cs₂BaTa₆Br₁₅O₃. *Chem. Eur. J.* **2013**, *19*, 12711–12719. [[CrossRef](#)]
39. Smakula, A.; Kalnajs, J. Precision Determination of Lattice Constants with a Geiger-Counter X-ray Diffractometer. *Phys. Rev.* **1955**, *99*, 1737–1743. [[CrossRef](#)]
40. Aghaei Hakkak, R.; Schleid, T. Low-Temperature Measurement of the Unexpected Hydrate Cs₂[B₁₂H₁₂]. *Acta Crystallogr.* **2023**, *A79*, in press.
41. Goto, A.; Hondoh, T.; Mae, S. The Electron Density Distribution in Ice I_h Determined by Single-crystal X-ray Diffractometry. *J. Chem. Phys.* **1990**, *93*, 1412–1417. [[CrossRef](#)]
42. Roobottom, H.K.; Jenkins, H.D.B.; Passmore, J.; Glasser, L. Thermochemical Radii of Complex Ions. *J. Chem. Educ.* **1999**, *76*, 1570–1573. [[CrossRef](#)]
43. Feldmann, C.; Jansen, M. Darstellung und Kristallstruktur von Cs₃ClO/Preparation and Crystal Structure of Cs₃ClO. *Z. Naturforsch.* **1995**, *50b*, 1415–1416. [[CrossRef](#)]
44. Feldmann, C.; Jansen, M. Zur kristallchemischen Ähnlichkeit von Aurid- und Halogenid-Ionen. *Z. Anorg. Allg. Chem.* **1995**, *621*, 1907–1912. [[CrossRef](#)]
45. Feldmann, C.; Jansen, M. Zur Kenntnis neuer ternärer Oxide mit anionischem Gold. *Z. Anorg. Allg. Chem.* **1995**, *621*, 201–206. [[CrossRef](#)]
46. Tiritiris, I.; Schleid, T.; Müller, K. Solid-State NMR Studies on Ionic *closo*-Dodecaborates. *Appl. Magn. Reson.* **2007**, *32*, 459–481. [[CrossRef](#)]
47. Zapata, F.; García-Ruiz, C. The Discrimination of 72 Nitrate, Chlorate and Perchlorate Salts Using IR and Raman Spectroscopy. *Spectrochim. Acta* **2018**, *A189*, 535–542. [[CrossRef](#)]
48. Klapötke, T.M. *Energetic Materials Encyclopedia*; de Gruyter: Berlin, Germany, 2018.
49. Sheldrick, G.M. *SHELXS-97 and SHELXL-97, Programs for Crystal Structure Solution and Refinement*; University of Göttingen: Göttingen, Germany, 1997.
50. Sheldrick, G.M. A Short History of SHELX. *Acta Crystallogr.* **2008**, *A64*, 112–122. [[CrossRef](#)]

Disclaimer/Publisher's Note: The statements, opinions and data contained in all publications are solely those of the individual author(s) and contributor(s) and not of MDPI and/or the editor(s). MDPI and/or the editor(s) disclaim responsibility for any injury to people or property resulting from any ideas, methods, instructions or products referred to in the content.